Corrosion Science 229 (2024) 111845

Contents lists available at ScienceDirect

Corrosion Science

journal homepage: www.elsevier.com/locate/corsci

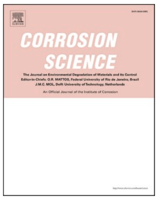

Monitoring alterations in a salt layer's deliquescence properties during the atmospheric corrosion of a metal surface using a quartz crystal microbalance

Arthur Situm [a], Mohammad Sabeti [a], November Schmidt [a], Dmitrij Zagidulin [a], Mehran Behazin [b], James J. Noël [a,*]

[a] *Department of Chemistry, Western University, London, ON, Canada*
[b] *Nuclear Waste Management Organization, Toronto, ON, Canada*

ARTICLE INFO

Keywords:
Atmospheric corrosion C
Sputtered films A
Copper A
XRD B
Oxidation C
Metal coatings A

ABSTRACT

The deliquescence of salt residues on metal structures can exacerbate the atmospheric corrosion of these structures. However, the conversion of salt residues to corrosion products alters the metal surface time of wetness (TOW) in ways that are difficult to monitor. This study demonstrates the use of quartz crystal microbalance with acoustic impedance measurement (QCM-I) to simultaneously monitor the corrosion and the changing deliquescence properties of various chloride salt layers printed on copper surfaces. While the results herein apply to Canada's proposed deep geological repository (DGR) for used nuclear fuel, the methodology applies to any combination of salts and metal surfaces.

1. Introduction

Within the study of atmospheric corrosion, the concept of time of wetness (TOW) is generally defined as the amount of time a metal surface remains wet during atmospheric exposure [1]. Of particular concern is the wetting of a metal surface resulting from the presence of deliquescent aerosols and salts, as this deliquescence can exacerbate the atmospheric corrosion of the metal. Limiting deliquescence-induced atmospheric corrosion of metal structures is a significant challenge impacting a variety of sectors, including marine transportation, potash mining, automotive, road transportation, bronze statuary, and radioactive waste storage [2–10]. As deliquescence-induced atmospheric corrosion progresses, the deliquescence properties of the salt-covered metal surface may be modified due to the development of corrosion products, which may or may not be deliquescent themselves. However, the role of corrosion products in determining the TOW of metal surfaces has received little attention [1].

One approach to studying atmospheric corrosion, deliquescence, and TOW is to use a quartz crystal microbalance (QCM) [11–13]. A QCM typically consists of an AT-cut quartz crystal, coated on both sides with conductive material that acts as electrodes [14,15]. The QCM possesses a known resonance frequency of the fundamental mode, which depends on the physical properties of the quartz crystal (e.g., ~6 MHz) [16,17]. The resonance frequency also can be derived from a measurement of the crystal's acoustic impedance, sometimes referred to as QCM with impedance measurement (QCM-I) [14,15]. Changes in resonance frequency (Δf) can be linearly proportional to the change in weight on the crystal's surface (Δm) under certain constraints [15,18]. This conversion between Δf and Δm is possible using the Sauerbrey equation, as shown in Eq. 1:[15,18].

$$\Delta f_N = \frac{2f_0^2}{A\sqrt{\rho_q \mu_q}} \Delta m \tag{1}$$

In Eq. 1, f_0 is the resonance frequency of the fundamental mode (Hz), Δf the change in resonance frequency (Hz), Δm the mass change (g), A the piezoelectrically active crystal area (cm^2), P_{q} the density of quartz (g/cm^3), and μ_{q} the shear modulus of quartz (g·cm^{-1}·s^{-2}) [15,18]. The use of the Sauerbrey equation is only valid if the mass on the crystal is rigidly attached and the film on the crystal is thin enough that the shift in resonance frequency is less than 2% of the initial resonance frequency [15,18].

Many studies have been conducted using QCM measurements to explore the atmospheric corrosion of various metals by monitoring the change in resonance frequency [13,19–24]. For example, the corrosion

---

* Corresponding author.
E-mail address: jjnoel@uwo.ca (J.J. Noël).

https://doi.org/10.1016/j.corsci.2024.111845
Received 6 October 2023; Received in revised form 4 December 2023; Accepted 11 January 2024

of copper by water vapors, sulphur dioxide, ozone, and nitrogen dioxide has previously been studied by Aastrup et al., and Aastrup and Leygraf, who used a combination of QCM measurements and infrared reflection absorption spectroscopy (IRAS) [13,23,24]. Furthermore, Forslund and Leygraf used QCM measurements to monitor TOW in situ in an outdoor environment. This was achieved by simultaneously measuring the deposition of aerosols on the QCM (measured as an irreversible change in resonance frequency) and water sorption (measured as a reversible change in resonance frequency dependent on changes in relative humidity (RH)).

Similarly, QCMs have previously been used to investigate the deliquescence of salt mixtures relevant to atmospheric chemistry by Arenas et al., and Chao et al. [12,25] The principle used in both studies relies on an effect seen in QCM measurements, where a salt that is rigidly attached to the surface of the QCM crystal dissolves once it undergoes deliquescence, leading to an abrupt increase in the resonance frequency measured [14]. Although the weight on the QCM crystal increases due to the deliquescence of the salt, once the salt is no longer rigidly attached to the surface of the crystal, its effect on suppressing the resonance frequency of the crystal is decreased [14].

While pure salts can have their deliquescence relative humidity (DRH) calculated from the thermodynamic properties of the salt, similar calculations for mixtures of salts can produce inaccurate results and require experimental validation to determine the mixtures' DRH [12,25]. Likewise, the efflorescence relative humidity (ERH), the RH at which the solution evaporates and leaves behind the solid salt, is also dependent on the kinetics of the water's evaporation and so must also be determined experimentally [12,25]. The separation of the DRH and the ERH as a result of evaporation kinetics is referred to as the "hysteresis effect" [12,25]. There are multiple techniques available for determining the DRH and ERH of a salt, which are reviewed in detail by Tang et al. [26] Of the techniques used for studying DRH and ERH, QCM possesses a high sensitivity in mass measurement, allowing individual monolayers of water on the surface of the QCM to be quantified [26]. However, the use of QCM as a technique for measuring the DRH and ERH in an outdoor environment is difficult due to the deposition of aerosol particles on the surface of the QCM crystal [11].

While monitoring changes in the resonance frequency of a quartz crystal is a powerful way of studying the atmospheric corrosion of metal surfaces and the deliquescence of salts, when these phenomena occur simultaneously on the surface of a QCM crystal, decoupling their effects on the resonance frequency is challenging [15]. However, it has been shown that in cases where salt on the surface of the crystal undergoes deliquescence, there is an abrupt increase in the resonance frequency, coupled to a simultaneous increase in the full-width at half maximum (FWHM) of the quartz crystal admittance [15]. When the salt is rigidly attached to the surface of the crystal, the acoustic wave passes through the salt inelastically, lowering the resonance frequency [15]. In contrast, when the salt is dissolved as a result of deliquescence, the acoustic wave no longer passes inelastically through the rigid salt but elastically through the brine [15]. The passing of the standing wave through bulk liquid results in a decay of the standing wave, which is observed as an increase in the FWHM of the admittance spectrum [15].

This present study aims to demonstrate a methodology to study the atmospheric corrosion of a salt-covered metal surface while simultaneously monitoring changes in the deliquescent properties of the surface under wet/dry cycling, using QCM-I. Copper was selected as the metal for this study, and a series of chloride salts were chosen as the deliquescent salts. Still, it should be emphasized that the methodology presented herein applies to any combination of salts and metal surfaces.

The motivation behind the choice of copper and chloride salts in this study stems from ongoing research related to Canada's plan for used nuclear fuel storage [3]. Many countries operating nuclear power plants are pursuing the strategy of sealing their used nuclear fuels in metallic containers and burying these containers deep underground in facilities known as deep geological repositories (DGRs) [3]. Canada is investigating different candidate sites and designs for a DGR that could involve using copper-coated carbon steel used fuel containers (UFCs), encased in highly compacted bentonite buffer boxes [3]. Following this emplacement, the environment around the containers will initially be aerobic and warm (~75 °C), while the bentonite surrounding the containers will not be saturated with water [3]. Accordingly, one of the issues being investigated is the initial atmospheric corrosion that could occur on the surface of the copper-coated UFC [3]. In particular, trace deliquescent chloride salt contaminants (e.g., NaCl, $MgCl_2$, and $CaCl_2$) deposited on a copper surface from bentonite may exacerbate the initial atmospheric corrosion of the copper coating. Thus, this study also provides initial insight into how the deliquescence behavior of these chloride salts deposited on copper will evolve as corrosion of the copper surface occurs.

2. Experimental

2.1. Magnetron sputtering of copper

Gold-coated QCM crystals (Au-QCM) were purchased from Inficon (6 MHz resonance frequency, 9 mm diameter). Copper-coated QCM crystals (Cu-QCM) were fabricated by coating Au-QCM crystals with a layer of copper with a thickness of 350 nm using an Edwards Auto500 magnetron sputtering instrument. The Cu target diameter was 3 in. and was purchased from Kurt J. Lesker. Argon was used as the working gas for the plasma generation with a flow of 14.5 mTorr, and a working pressure was 1×10^{-8} bar. The distance between the target and the substrate was 10.7 cm, and a discharge power of 150 W was used. We performed pre-deposition sputtering for 10 min before exposing the Au-QCM crystals, to remove any contaminants from the surface of the Cu target. The deposition rate was 20.7 nm/min, and a coating with a thickness of 350 nm was achieved after 17 min of deposition. A mask was used to cover a small portion of each Au-QCM crystal to prevent copper deposition, with this small potion acting as the contact point for QCM-I measurements.

2.2. Printing of salt films using an inkjet printer

Different salts were printed onto the QCM crystals using an Epson XP-970 inkjet piezoelectric printer utilizing aftermarket refillable cartridges and the printer's CD ROM printing capability. The amount of salt dispensed by using the printer cartridge slots associated with each color type (i.e., black, yellow, magenta, and cyan) was determined by printing a 0.5 M NaCl (Fisher, 99%) solution onto Au-QCM crystals and using QCM-I and the Sauerbrey equation to determine the weight of NaCl printed on the piezoelectrically active area of the Au-QCM crystal ($1.02\ cm^2$). A detailed description of this process and the use of the Epson XP-970 for salt printing can be found in the supplemental information (SI). These measurements determined that printing from the 0.5 M NaCl cartridge resulted in 0.67 μmol of NaCl printed from the black cartridge slot, while the average mass using the yellow, magenta, and cyan cartridge slots was 0.24 μmol. This result was used to determine the concentration of salt solutions required to be made in the printer cartridges when printing on the QCM crystals in this study.

Printing of NaCl, $CaCl_2$ (from $CaCl_2 \cdot 2\,H_2O$, Caledon, 99%), and $MgCl_2$ solutions (from $MgCl_2 \cdot 6\,H_2O$, EDM, 99%) onto QCM crystals was performed such that 0.48 μmol of Cl was deposited on the $1.02\ cm^2$ piezoelectrically active area of the QCM crystal (i.e., $27.5\ \mu g/cm^2$ NaCl, $26.1\ \mu g/cm^2$ $CaCl_2$, and $22.4\ \mu g/cm^2$ $MgCl_2$). Salts were printed onto QCM crystals such that most of each crystal's surface was covered, except for a small portion acting as the contact point for QCM-I measurements. A solution with a mixture of salts was also printed onto the QCM crystals, referred to as CR-10E. The composition of CR-10E (Table 1) is a crystalline Canadian reference groundwater in equilibrium with bentonite clay. CR-10E was printed four times on the same surface, resulting in 0.33 μmol of Cl being deposited on each QCM

Table 1
Shows the composition of CR-10E, which is a crystalline Canadian reference groundwater in equilibrium with bentonite clay [37].

Solute	mg/L	mM
Na^{+}	1899	82.60
K^{+}	15	0.38
Mg^{2+}	60	2.5
Ca^{2+}	2217	55.32
$HCO3^{-}$	50	0.82
SO_4^{2-}	1243	12.94
Cl^{-}	6099	171.9
Sr^{2+}	25	0.29
F^{-}	2	0.1
Si	5	0.2
NO_3^{-}	1	0.02
PO_4^{3-}	1	0.01

crystal's piezoelectrically active area (i.e., 11.5 μg/cm^2 Cl). Salts were printed within the open laboratory environment, with NaCl and CR-10E drying within a minute of being printed, while $CaCl_2$ and $MgCl_2$ took around 2 min to dry after being printed. SEM images of NaCl, $CaCl_2$, $MgCl_2$, and CR-10E printed on the surface of QCM crystals are shown in Fig. S1.

2.3. Quartz crystal microbalance setup

All experiments were conducted within a humidity chamber (Associated Environmental Systems BHD-405 benchtop humidity chamber) to provide the relative humidity needed to simulate a corrosive environment. The holder for the QCM crystals was custom-made using a gold wire as the contact point to the gold contacts on the QCM crystals. QCM-I measurements were performed using an Agilent E5100A network analyzer controlled by a custom LabVIEW program to extract resonance frequency and FWHM values from the admittance spectrum simultaneously. In this study, the change in resonance frequency (Δf) was made relative to the resonance frequency at the start of the experiment (i.e., at t = 0 the $\Delta f = 0$).

2.4. QCM-I measurements

Two types of experiments were conducted in this study: salt deliquescence experiments to determine the DRH and ERH of individual salts and salt mixtures, and corrosion experiments to show how the TOW, DRH and ERH change with the formation of corrosion products. Salt deliquescence experiments were performed using salt-printed Au-QCM crystals at both 75 °C and 25 °C. Such experiments were conducted by raising the RH gradually from 3% to 90% and back to 3% linearly, in a continuous fashion, over 30 h. Corrosion experiments were conducted on salt-printed Cu-QCM crystals by maintaining a temperature of 75 °C and varying the RH from 3% to 90% in 5 wet/dry cycles over the course of 165 h. Following corrosion experiments, Cu-QCM crystals were stored in a desiccator, and optical microscope images were collected using a Keyence VHX-6000 Digital Microscope.

The Sauerbrey equation (Eq. 1) can be used to measure the weight gain of QCM crystals when the RH is at 3%. The constant parameters within the Sauerbrey equation are related to the properties of the QCM crystal used in the experiment; ρ_q is the density of quartz (2.648 g·cm^{-3}), μ_q the shear modulus of quartz (2.947 ×1011 g·cm^{-1}·s^{-2}), f_0 the resonant frequency of the fundamental mode (5.986 MHz), and A the piezoelectrically active crystal area (1.02 cm^2).

2.5. Grazing incidence X-ray diffraction measurements

Grazing incidence X-ray diffraction (GI-XRD) measurements were conducted at Surface Science Western (SSW) at Western University, London, Ontario, Canada. GI-XRD was conducted on Cu-QCM crystals, following corrosion testing, using a Rigaku SmartLab equipped with a Cu anode. GI-XRD peak identification was performed using Rigaku's SmartLab Studio II utilizing the PDF-4 + Database, the Crystallography Open Database (COD), and the FIZ/NIST Inorganic Crystal Structure Database (ICSD).

3. Results and discussion

3.1. Effect of humidity on the resonance frequency and FWHM of QCM-I measurements

To demonstrate the effect RH has on the QCM-I measurements, we performed a control experiment in which an Au-QCM crystal was subjected to increasing RH at 75 °C, the results of which are shown in Fig. 1. Fig. 1a demonstrates how the Δf gradually decreases as the RH is increased, due to water adsorption on the surface of the Au-QCM crystal. This is the same principle used by Forslund and Leygraf when demonstrating the use of a QCM crystal as a TOW sensor.[11] In contrast, Fig. 1b demonstrates how the FWHM remains almost constant until the RH reaches 100%, at which point the FWHM value dramatically increases. This result demonstrates the sensitivity of QCM-I FWHM measurement to the presence of water and thus deliquescence.

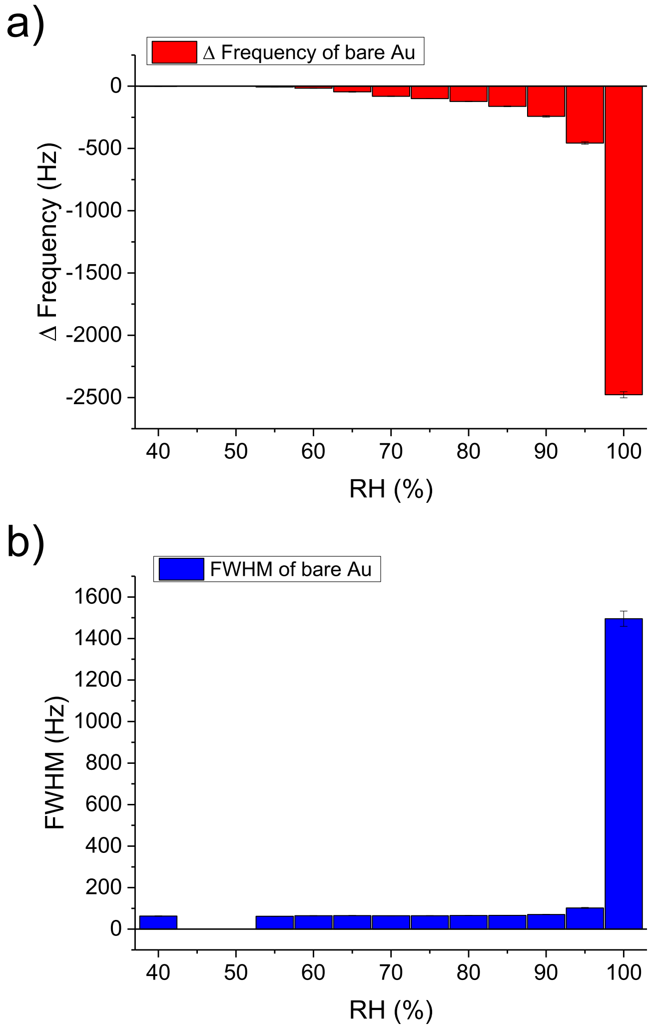

Fig. 1. a) Δf and b) FWHM response as a function of RH for a Au-coated QCM crystal at 75 °C. Each RH level was held for one hour.

3.2. Deliquescence of chloride salts

The deliquescence and efflorescence properties of NaCl, $CaCl_2$, $MgCl_2$, and CR10-E were tested to determine their DRH and ERH points. The Δ*f* and FWHM results for NaCl, $CaCl_2$, $MgCl_2$, and CR-10E printed on Au-QCM crystals vs RH at 75 °C and 25 °C are shown in Fig. 2 and Fig. S2, respectively. Figs. 2a and 2b show that when the RH reaches 75%, the Δ*f* and FWHM sharply increase as the NaCl deliquesces and decrease sharply when the RH is lowered to 63% and the NaCl effloresces. This increase in Δ*f* is attributed to the NaCl no longer being rigidly attached to the surface of the QCM crystal, overcoming the drop in Δ*f* due to the added weight from the water. In contrast to the deliquescence behavior of NaCl, Figs. 2c and 2d show that $CaCl_2$ demonstrated a sharp increase in Δ*f* and FWHM at 20% RH, corresponding with deliquescence, but no sharp decrease in FWHM associated with efflorescence, since the rate increased as the RH decreased. While the small but sharp decreases in Δ*f* as the RH was increased up to 20% suggest that $CaCl_2$ is hydrating to form $CaCl_2{\cdot}2\ H_2O$ and potentially $CaCl_2{\cdot}4\ H_2O$, the sharp increase in Δ*f* as the RH was decreased to 14% does not correspond with a sharp decrease in FWHM, indicating that the $CaCl_2$ had not finished efflorescing until about 7% RH, when the FWHM stopped decreasing and returned to the initial value of 120 Hz. It should also be noted that differences in Δ*f* at the start and end of the experiment (at the end of the experiment Δ*f* = *900 Hz)* may have been due to a salt redistribution on the crystal or a difference in the hydration state of the $CaCl_2$ compared with the state at t = 0, neither of which affects FWHM measurements. These results demonstrate the superiority of using FWHM QCM-I measurements for monitoring deliquescence over relying only on Δ*f* measurements.

The advantage of monitoring FWHM to track deliquescence behavior was further demonstrated by QCM-I measurements conducted on $MgCl_2$ and CR10-E printed films. Figs. 2e and 2 f show that, while the sharp decrease in Δ*f* that occurred when the RH was increased to 13% suggests hydration of the $MgCl_2$, the sharp increase in FWHM indicates that a portion of the $MgCl_2$ had deliquesced and dissolved. Furthermore, Fig. 2 g and 2 h show small but sharp increases and decreases in Δ*f* and FWHM, indicating deliquescence occurs above 18% RH while efflorescence occurs below 7.5% RH.

A summary of DRH and ERH values measured for NaCl-, $CaCl_2$-, $MgCl_2$-, and CR-10E-coated Cu surfaces at 75 °C and 25 °C is shown in Table 2. Although a DRH of 75% for NaCl is similar to results from previous studies, the ERH measured in this study (63% RH) is higher than the NaCl ERH value measured by Zeng et al. (48% RH at 23 °C) [27–29]. Unlike DRH, which is a property governed by thermodynamics, ERH is a kinetically controlled parameter. The hysteresis effect observed between deliquescence and efflorescence is attributed to the lack of nucleation seeds in pure NaCl solution [27]. Thus, it is possible that the NaCl was able to effloresce at 63% RH in our work due to the presence of a trace contaminant, which, perhaps, represents a more realistic ERH for NaCl in a natural system. $CaCl_2$, $CaCl_2{\cdot}2\ H_2O$, $CaCl_2{\cdot}4\ H_2O$, and $CaCl_2{\cdot}6\ H_2O$ were previously reported to have DRHs of 27–32%, 18–19%, 23%, and 28–29%, respectively, at 23 °C [28]. Gough et al. have previously reported that above -20 °C, $CaCl_2{\cdot}2\ H_2O$ undergoes deliquescence (i.e., $CaCl_2{\cdot}4\ H_2O$, and $CaCl_2{\cdot}6\ H_2O$ do not form) and is observed to have an ERH of 3.5% at 0 °C [30]. The DRH of 20% at both 25 °C and 75 °C found in this study are in line with the presence of $CaCl_2{\cdot}2\ H_2O$. Peng et al. previously found that, at 23 °C, $MgCl_2$, $MgCl_2{\bullet}4\ H_2O$ and $MgCl_2{\cdot}6\ H_2O$ had DRH values of 31–35%, 15–17%, and 30–35%, respectively, as well as ERH values of < 1.5%, 6–8%, and 9–11%, respectively [28]. In this study, two different DRHs were detected for the $MgCl_2$ printed film sample, one of which likely corresponds to the deliquescence of $MgCl_2{\bullet}4\ H_2O$ (15% RH at 25 °C), while the other may correspond to the deliquescence of $MgCl_2$ or $MgCl_2{\cdot}6\ H_2O$ (31% RH at 25 °C) [28,29]. Finally, unlike the salt mixtures previously studied using QCM, CR-10E was not observed to have a defined DRH corresponding with a eutectic mixture [12,25]. The lack of a eutectic DRH for CR-10E may result from the presence of salts in various hydration states and with several DRH values.

3.3. Atmospheric corrosion of copper by chloride salts during wetting and drying cycles

QCM-I was performed on a Cu-QCM crystal without any printed salts (bare Cu-QCM crystal) under wet/dry cycling at 75 °C with the measured Δ*f* and FWHM vs experimental time shown in Fig. 3. Fig. 3a shows that over the course of all wet/dry cycles, Δ*f* decreased; this decrease is attributed to the atmospheric corrosion of the copper coating increasing the weight of the coating. Additionally, within every wet/dry cycle (RH shown in black), Δ*f* fluctuated, showing a small increase when the RH was increasing and decreasing as the RH decreased, which is partially attributable to the adsorption and desorption of water from the crystal's surface. From Fig. 3b, we see that the FWHM of the bare Cu-QCM crystal fluctuated by ~15 Hz in response to the changes in RH, with most of the increase occurring when the RH approached 90%. The fluctuation in FWHM recorded on the bare Cu-QCM crystal was far smaller than were the changes in FWHM resulting from the deliquescence of salts on the surface of the Au-QCM crystal (see Fig. 2).

QCM-I was performed on a Cu-QCM crystal with printed layers of salts under wet/dry cycling at 75 °C to test the effectiveness of using QCM-I FWHM measurements in studying the changing deliquescence properties of salt-covered crystal surfaces. QCM-I results obtained from a Cu-QCM crystal with a printed film of NaCl (NaCl-Cu-QCM crystal), along with GI-XRD patterns collected from the corroded copper coating, are shown in Fig. 4. From the Δ*f* plot of the NaCl-printed Cu-QCM crystal (Fig. 4a), we observed that the copper surface continued to deliquesce and effloresce during wet/dry atmosphere cycles for the entire week. However, the value of Δ*f* when the crystal was dry varied without following any specific trend. The variation in Δ*f*, when the NaCl-Cu-QCM crystal was dry, likely results from the redistribution of the NaCl during every wet/dry cycle, with more or less of the solid precipitating onto (vs outside) the piezoelectric active area of the QCM crystal. While this variation in Δ*f* prevents the quantification of the corrosion of the NaCl-Cu-QCM crystal, information can still be obtained from the FWHM results shown in Fig. 4b. A sharp rise in the FWHM was observed when the RH was increased to 75%, in line with the known DRH of NaCl. However, a sharp decrease in FWHM was observed when the RH was decreased to 73%; i.e., the efflorescence of NaCl occurred at a RH value higher than the ERH value found during deliquescence testing using a Au-QCM crystal (see Table 2). Since efflorescence is a kinetically determined process, it's possible that the development of corrosion products created a copper surface that was more favorable to efflorescence, thus increasing the observed ERH. Additionally, we observed an increase in the maximum FWHM from ~600 to ~1100 Hz after multiple wet/dry cycles when NaCl was printed on a Au-QCM; this is thus not likely to be a result of corrosion (see Fig. S3).

GI-XRD patterns collected from the NaCl-Cu-QCM crystal following wet/dry cycling indicated the presence of paratacamite ($Cu_2(OH)_3Cl$) and tenorite (CuO) (see Fig. 4c). While the formation of paratacamite and clinoacamite (another $Cu_2(OH)_3Cl$ polymorph) following NaCl-induced atmospheric corrosion of copper at room temperature has been observed previously, to the best of the authors' knowledge, the present study is the first performed at an elevated temperature [31–34]. Additionally, no sodium-containing crystalline phase, aside from NaCl, was detected; this is in line with the findings of Strandberg and Johansson [31].

QCM-I results obtained from a Cu-QCM crystal with a printed film of $CaCl_2$ ($CaCl_2$-Cu-QCM crystal), along with GI-XRD patterns collected from the corroded copper coating following wet/dry cycling, are shown in Fig. 5. In contrast to the NaCl-Cu-QCM crystal, the $CaCl_2$-Cu-QCM crystal underwent limited deliquescence that quickly ceased, as evidenced by the sharp increase in FWHM from 90 to 280 Hz followed by a sharp decrease to 75 Hz once the RH reached 50% during the first wet

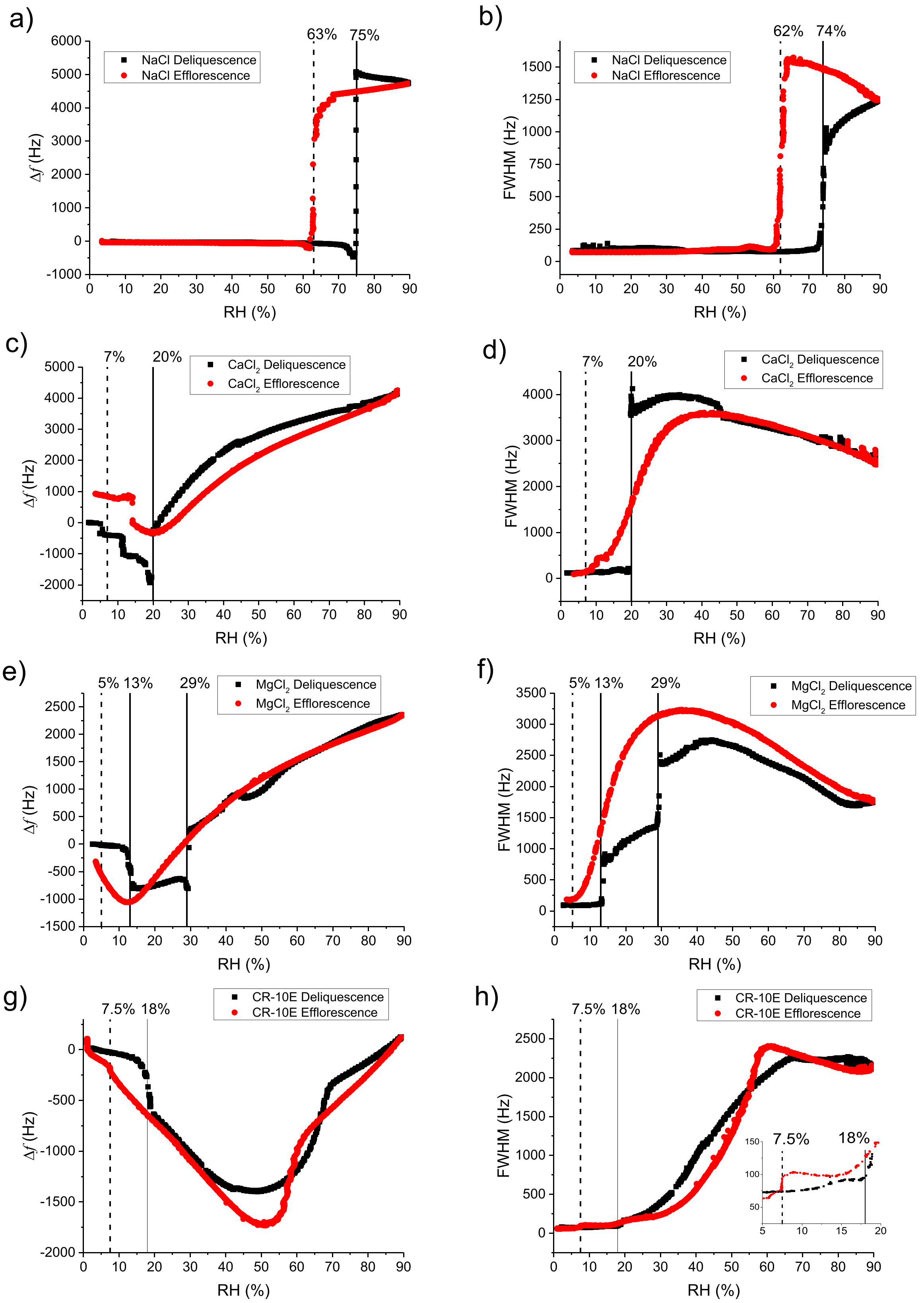

Fig. 2. a), c), e), g) Δf and b), d), f), h) FWHM response as a function of RH for NaCl, $CaCl_2$, $MgCl_2$, and CR-10E printed on an Au-coated QCM crystal at 75 °C, respectively. The black symbols indicate the period of the experiment during which the RH was gradually scanned over 15 h, while the red symbols indicate when the RH was gradually decreased over 15 h.

Table 2
DRH and ERH values were determined for various salt films on the surface of a gold-coated QCM crystal.

	DRH at 75 °C	ERH at 75 °C	DRH at 25 °C	ERH at 25 °C
NaCl	75%	63%	75%	63%
$CaCl_2$	20%	~7%	17–20%	~6%
$MgCl_2$	13–29%	~5%	15–31%	~7%
CR-10E	>18%	<7.5%	>14%	<11%

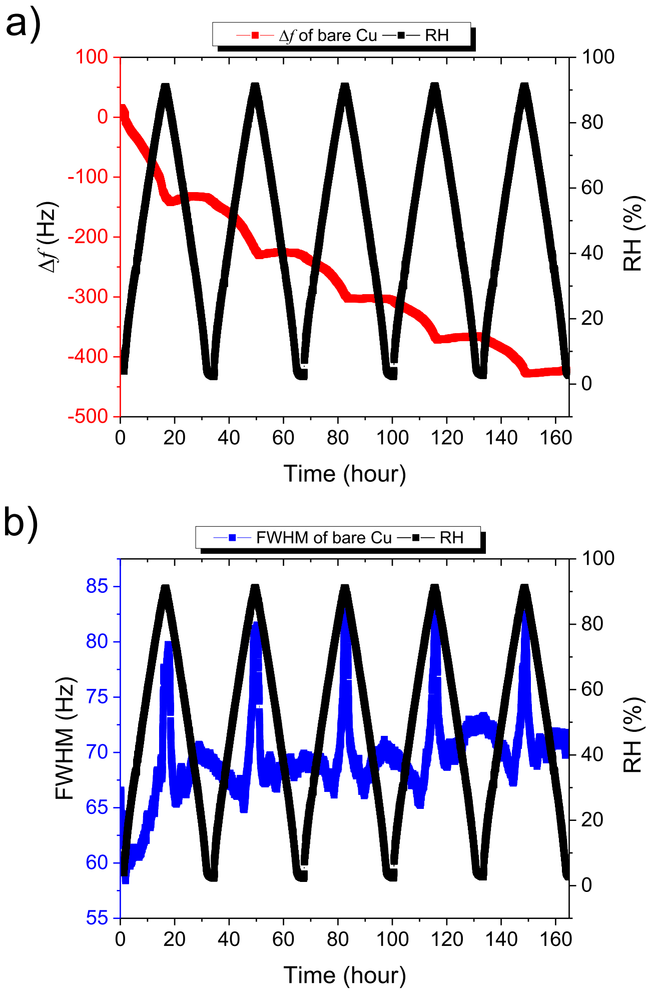

Fig. 3. a) Δ*f* and b) FWHM response as a function of time for a Cu-coated QCM crystal. The temperature of the humidity chamber was held at 75 °C while the RH was cycled between 3% and 90%.

cycle (see Fig. 5b). Moreover, the FWHM did not increase above 100 Hz for the remainder of the experiment; once deliquescence was lost, it did not return (see Fig. 5). GI-XRD results indicate the presence of centennialite ($CaCu_3Cl_2(OH)_6{\cdot}nH_2O$ (n ~ 0.7)), which is not deliquescent. The formation of centennialite likely explains why deliquescence was lost so quickly, with the originally deliquescent $CaCl_2$ being converted into the non-deliquescent corrosion product. A similar effect was found for a Cu-QCM crystal with a printed film of $MgCl_2$ ($MgCl_2$-Cu-QCM crystal). QCM-I results obtained from a $MgCl_2$-Cu-QCM crystal, along with GI-XRD patterns collected from the corroded copper coating following wet/dry cycling, are shown in Fig. 6. The FWHM values recorded on the $MgCl_2$-Cu-QCM crystal indicate that deliquescence was also lost, with the FWHM being < 30 Hz during the final wet/dry cycle (see Fig. 6b). GI-XRD results indicate the presence of haydeeite ($Cu_3Mg(OH)_6Cl_2$), a non-deliquescent corrosion product, following wet/dry cycling of the $MgCl_2$-Cu-QCM crystal, which explains the loss of deliquescence.

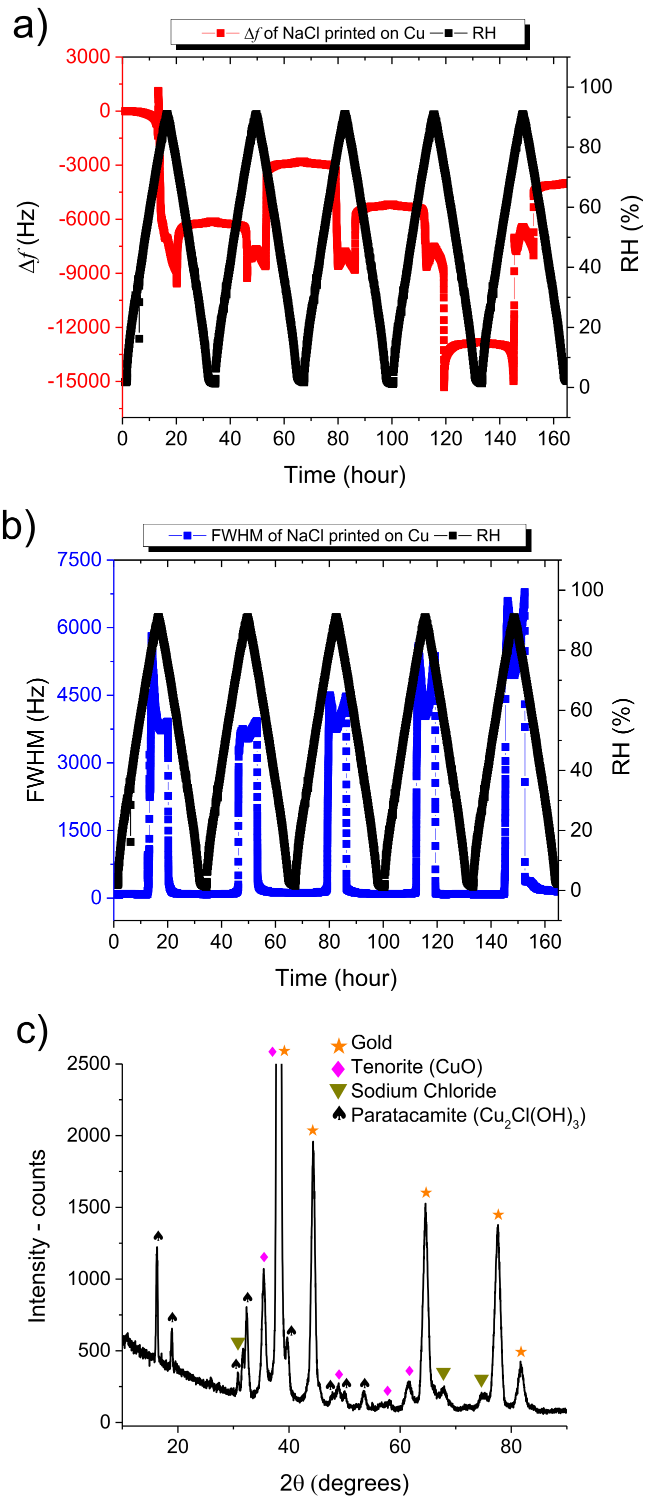

Fig. 4. a) Δ*f* and b) FWHM response as a function of time for NaCl printed on a Cu-coated QCM crystal (NaCl-Cu-QCM). The temperature of the humidity chamber was held at 75 °C while the RH was cycled between 3% and 90%. c) GI-XRD pattern collected following corrosion testing for 165 h.

QCM-I results obtained from a Cu-QCM crystal with a printed film of CR-10E (CR-10E-Cu-QCM crystal), along with GI-XRD patterns collected from the corroded surface following wet/dry cycling, are shown in Fig. 7. The Δ*f* and FWHM results obtained from the CR-10E-Cu-QCM

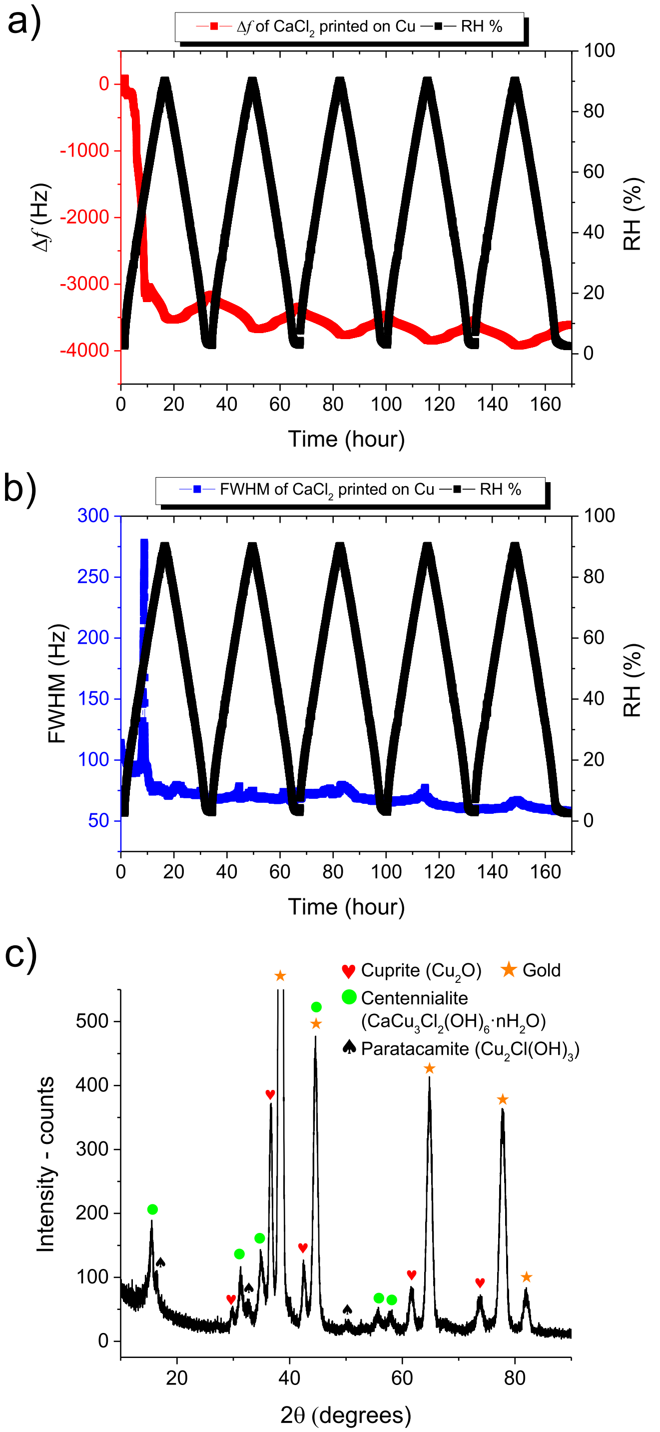

Fig. 5. a) Δ*f* and b) FWHM response as a function of time for $CaCl_2$ printed on a Cu-coated QCM crystal ($CaCl_2$-Cu-QCM). The temperature of the humidity chamber was held at 75 °C while the RH was cycled between 3% and 90%. c) GI-XRD pattern collected following corrosion testing for 165 h.

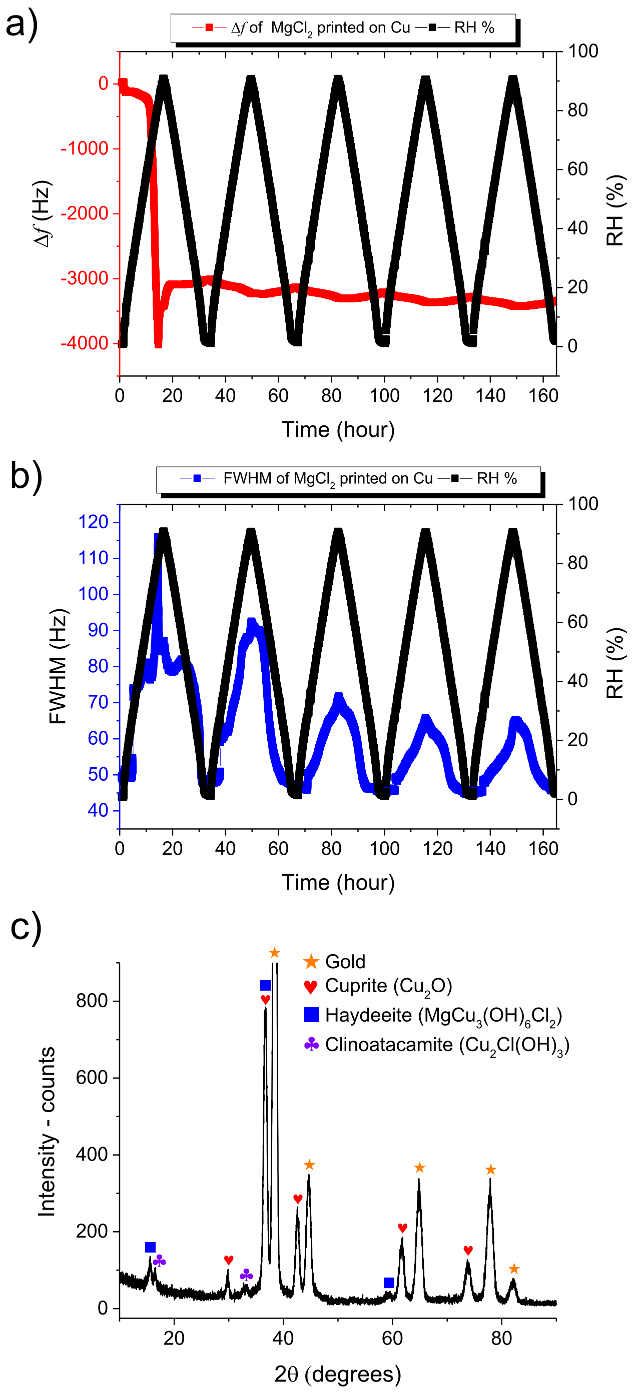

Fig. 6. a) a) Δ*f* and b) FWHM response as a function of time for $MgCl_2$ printed on a Cu-coated QCM crystal ($MgCl_2$-Cu-QCM). The temperature of the humidity chamber was held at 75 °C while the RH was cycled between 3% and 90%. C) GI-XRD pattern collected following corrosion testing for 165 h.

crystal show some similarities to the results from the NaCl-Cu-QCM crystal, with no traces of deliquescence from $CaCl_2$ or $MgCl_2$, indicating that both $CaCl_2$ or $MgCl_2$ were converted to non-deliquescent corrosion products during the initial wetting phase. However, GI-XRD results collected from the CR-10E-Cu-QCM crystal following wet/dry cycling do not indicate the presence of centennialite or haydeeite but rather clinoacamite, indicating that $CaCl_2$ or $MgCl_2$ may have been converted into other non-deliquescent corrosion products (e.g., $Ca(OH)_2$ and $Mg(OH)_2$). Additionally, the magnitude of the Δ*f* measured when the CR-10E-Cu-QCM crystal was dry increased with each wet/dry cycle (see Fig. 7a), unlike that of the NaCl-Cu-QCM, which showed a considerable variation, potentially due to NaCl redistribution on the surface between wet/dry cycles. While it is not the focus of this study, the corrosion of the Cu coating can be quantified based on the decrease in resonance frequency when the crystal is dry (e.g., at 3% RH) using the Sauerbrey equation (see Eq. 1). For instance, comparing the Δ*f* values collected from the CR-10E-Cu-QCM crystal at the second last and last points where the RH was 3% (i.e., at 132 h and 165 h), there was a decrease in resonance frequency of 140 Hz, which corresponds to a

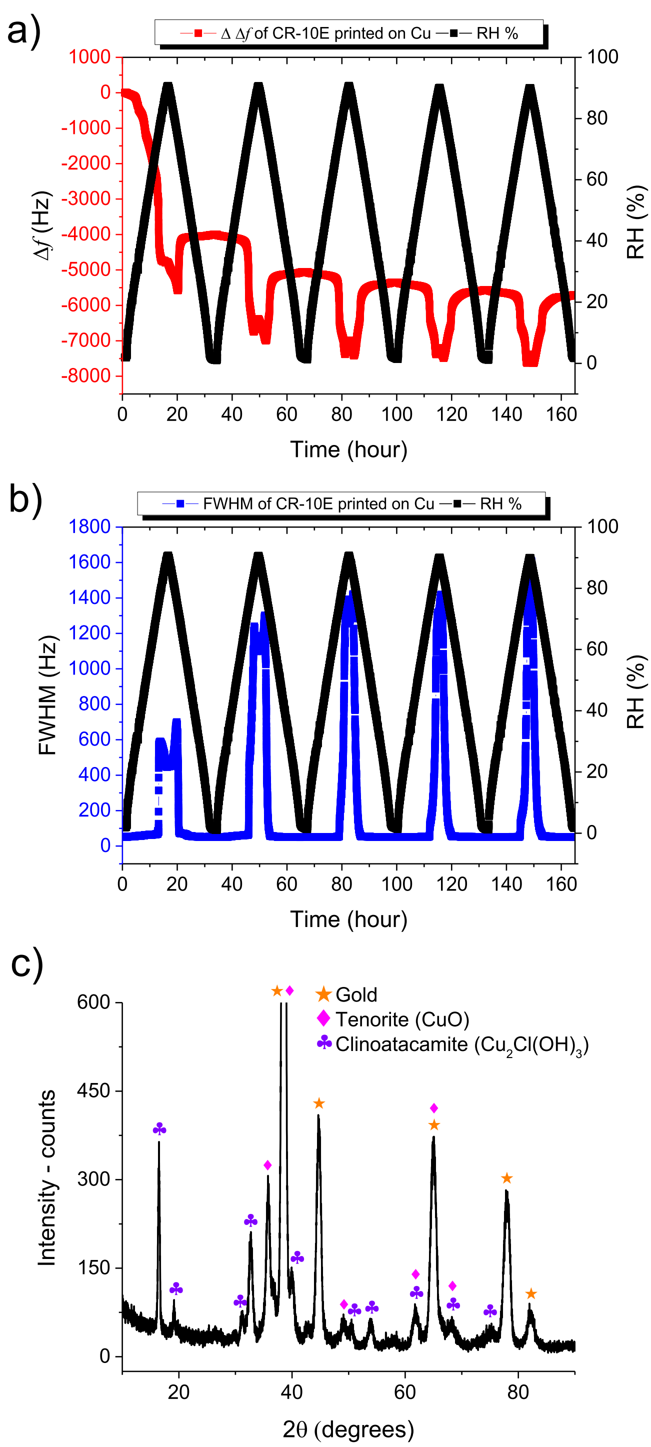

Fig. 7. a) Δ*f* and b) FWHM response as a function of time for CR-10E printed on a Cu-coated QCM crystal (CR-10E-Cu-QCM). The temperature of the humidity chamber was held at 75 °C while the RH was cycled between 3% and 90%. c) GI-XRD pattern collected following corrosion testing for 165 h.

weight gain on the copper over the piezoelectric active area of 1.77 μg. An upcoming publication will use the Sauerbrey equation to analyze the deliquescence-induced atmospheric corrosion behavior of Cu coatings.

While the FWHM measurements obtained from the CR-10E-Cu-QCM crystal initially resembled those of the NaCl-Cu-QCM crystal, the FWHM peaks indicating deliquescence shifted over time to higher RH values. Fig. 8 shows the FWHM measurements taken from the CR-10E-Cu-QCM crystal during the first and final wet/dry cycles. During the first wet/dry cycle, a sharp increase in FWHM occurred when the RH was increased to 75% RH, corresponding with the DRH of NaCl, while an ERH of 73–70% was observed (see Fig. 8a). However, by the final wet/dry cycle, there was only a slight increase in FWHM when the RH was increased to 75% (55 to 130 Hz), whereas a gradual but more significant increase in FWHM was observed at 80–85% RH, with the FWHM reaching ~1600 Hz (see Fig. 8b). Additionally, the FWHM was observed to decrease gradually during the final wet/dry cycle as the RH was lowered (see Fig. 8b). These results indicate that much of the NaCl was converted to a corrosion product that deliquesces at a higher RH than does NaCl. Using in situ Fourier transform infrared (FTIR) microscopy measurements, Chen et al. previously observed the formation of a carbonate-containing compound when a copper specimen with a single NaCl particle was exposed to air at ~80% RH with a CO_2(g) content of 350 ppm [35]. The identity of this carbonate-containing species was thought to be Na_2CO_3 which is known to have a DRH of 85% [35,36]. Moreover, similar experiments using FTIR microscopy, conducted by the authors at 75 °C, have shown the formation of $NaHCO_3$; the results of these experiments will be the subject of an upcoming publication.

The deliquescence properties of Na_2CO_3 and $NaHCO_3$ were measured by placing loose particles of these compounds on Au-QCM crystals and performing wet/dry cycling at 75 °C (FWHM results shown in Fig. S4). Na_2CO_3 was observed to have a DRH of 85% and an ERH of 74%, while $NaHCO_3$ was observed to have a DRH of ~82% and no ERH. While these results suggest that the NaCl on the CR-10E-Cu-QCM crystal may have been converted to $NaHCO_3$ and clinoacamite, FTIR microscopy performed on the CR-10E-Cu-QCM crystal did not detect the presence of carbonate (see Fig. S5). These results suggest that FWHM measurements made using QCM-I have the ability to detect deliquescent corrosion products that would otherwise go undetected by characterization techniques such as XRD and FTIR.

The formation of clinoacamite and other non-deliquescent copper corrosion products containing Cl has implications for the performance of UFCs in a DGR, as the formation of these species may act as a stifling mechanism for corrosion resulting from chloride-containing impurities on the UFC surface, by consuming available chloride anions, metal cations, and water and decreasing the TOW. The deposition of such mineralized films on UFC surfaces also introduces a possible mechanism for localizing subsequent corrosion damage at sites where the mineralized layer cracked or did not form, but this form of localization differs substantially from classical localized corrosion processes, as the latter requires an electronically conducting passive film that supports the cathodic half-reaction, whereas these mineralized films should be electronically insulating, working by a barrier effect only.

The formation of chloride-containing non-deliquescent copper corrosion products under DGR-relevant conditions is the subject of ongoing research which will utilize the methodology presented herein to monitor changes in the deliquescence properties of salt-covered copper surfaces. Overall, this study demonstrates how FWHM measurements obtained from QCM-I can be used to monitor the deliquescence properties of a salt-covered corroding metal surface, complementing atmospheric corrosion experiments.

4. Summary and conclusions

- This study demonstrated the use of QCM-I to monitor the atmospheric corrosion of a salt-covered metal surface while simultaneously monitoring changes in the deliquescent properties of the surface during wet/dry cycling. While chloride salts and copper metal were chosen to demonstrate the use of QCM-I to study the changing deliquescence properties of salt-covered metal surfaces, this methodology is applicable to any combination of salt and metal.
- FWHM measurements of the acoustic impedance response can be used to monitor the deliquescence properties of the salt-covered corroding metal surface, independent of weight changes resulting from corrosion.

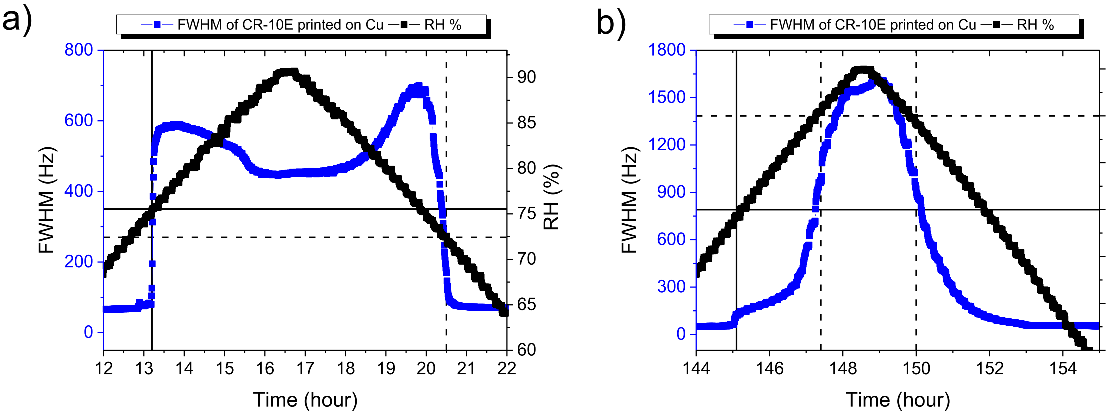

Fig. 8. Select FWHM measurements made during corrosion testing of the QCM crystal described in Fig. 7 (CR-10E-Cu-QCM). a) FWHM measurements between 12 and 22 h of corrosion testing. b) FWHM measurements between 144 and 155 h of corrosion testing. The complete plot of FWHM measurements taken during corrosion testing is presented in Fig. 7b.

- The Sauerbrey equation can be used to quantify the weight gain of the metal surface by measuring the change in resonance frequency, but only when the surface of the QCM crystal is dry and any salt residue on the metal surface is not redistributed outside of the piezoelectric active area when the surface of the QCM crystal is wet.
- $CaCl_2$ and $MgCl_2$ printed on Cu-coated QCM crystals were observed to lose deliquescence properties rapidly. This loss of deliquescence was attributed to the formation of centennialite ($CaCu_3Cl_2(OH)_6 \cdot nH_2O$) and haydeeite ($MgCu_3(OH)_6Cl_2$) from the printed $CaCl_2$ and $MgCl_2$, respectively.
- The CR-10E mixture printed on Cu-coated QCM crystals was observed to undergo a shift in its DRH from a value near that of NaCl to higher RH values incrementally during repeated wet/dry cycles. This shift in deliquescence was attributed to the conversion of NaCl into clinoacamite ($Cu_2Cl(OH)_3$) and $NaHCO_3$.

CRediT authorship contribution statement

Noël James J: Conceptualization, Funding acquisition, Methodology, Project administration, Resources, Supervision, Validation, Writing – review & editing. **Behazin Mehran:** Conceptualization, Funding acquisition, Project administration, Writing – review & editing. **Zagidulin Dmitrij:** Formal analysis, Methodology, Software. **Schmidt November:** Investigation. **Sabeti Mohammad:** Investigation. **Situm Arthur:** Conceptualization, Data curation, Formal analysis, Investigation, Methodology, Visualization, Writing – original draft, Writing – review & editing.

Declaration of Competing Interest

The authors declare the following financial interests/personal relationships which may be considered as potential competing interests: James J. Noel reports financial support was provided by Natural Sciences and Engineering Research Council of Canada. James J. Noel reports financial support was provided by Nuclear Waste Management Organization. James J. Noel reports a relationship with Nuclear Waste Management Organization that includes: funding grants. James J. Noel reports a relationship with Natural Sciences and Engineering Research Council of Canada that includes: funding grants. Mehran Behazin reports a relationship with Nuclear Waste Management Organization that includes: employment. Arthur Situm reports a relationship with Natural Sciences and Engineering Research Council of Canada that includes: funding grants. If there are other authors, they declare that they have no known competing financial interests or personal relationships that could have appeared to influence the work reported in this paper.

Data availability

Raw data used in this publication can be accessed here: https://doi.org/10.5683/SP3/3AY7MY. Processed data used in this publication can be accessed here: https://doi.org/10.5683/SP3/OKKDZD.

Acknowledgements

This work was jointly funded by the Natural Sciences and Engineering Research Council of Canada (NSERC) and the Nuclear Waste Management Organization through Alliance Grant ALLRP561193-20. We gratefully acknowledge Tim Goldhawk and Todd Simpson at the Western Nanofabrication facility for sample preparation. We also gratefully acknowledge Thalia Standish, Mya Caverson and Vahid Dehnavi for their help with FTIR and GI-XRD measurements at Surface Science Western.

Appendix A. Supporting information

Supplementary data associated with this article can be found in the online version at doi:10.1016/j.corsci.2024.111845.

References

[1] E. Schindelholz, R.G. Kelly, Wetting phenomena and time of wetness in atmospheric corrosion: a review, Corros. Rev. 30 (2012) 135–170, https://doi.org/10.1515/corrrev-2012-0015.

[2] E. Schindelholz, B. Risteen, R. Kelly, Effect of relative humidity on corrosion of steel under sea salt aerosol proxies: II. MgCl2, artificial seawater, J. Electrochem. Soc. 161 (2014) C460–C470, https://doi.org/10.1149/2.0231410jes.

[3] D.S. Hall, M. Behazin, W. Jeffrey Binns, P.G. Keech, An evaluation of corrosion processes affecting copper-coated nuclear waste containers in a deep geological repository, Prog. Mater. Sci. 118 (2021) 100766, https://doi.org/10.1016/j.pmatsci.2020.100766.

[4] E. Schindelholz, B. Risteen, R. Kelly, Effect of relative humidity on corrosion of steel under sea salt aerosol proxies: I. NaCl, J. Electrochem. Soc. 161 (2014) C450–C459, https://doi.org/10.1149/2.0221410jes.

[5] A. Situm, X. Guo, B.C. Barlow, B. Guo, I.J. Burgess, A.P. Grosvenor, A spectromicroscopy study of the corrosion of polymer coated steel, Corros. Sci. 145 (2018) 35–46, https://doi.org/10.1016/j.corsci.2018.09.008.

[6] B.C. Barlow, A. Situm, B. Guo, X. Guo, A.P. Grosvenor, I.J. Burgess, X-ray microprobe characterization of corrosion at the buried polymer-steel interface, Corros. Sci., 144 (2018) 198–206. https://doi.org/10.1016/j.corsci.2018.08.051. https://www.sciencedirect.com/science/article/pii/S0010938×18312459.

[7] R. Legault, V. Pearson, Atmospheric corrosion in marine environments, Corrosion 34 (1978) 433–437, https://doi.org/10.3390/ma10040406.

[8] C. Houska, Deicing salt–recognizing the corrosion threat, International Molybdenum Association, Pittsburgh, TMR Consulting, (2007) 1–10. doi: 10.1002/maco.201709907.

[9] Ž. Novak, T. Kosec, Corrosion and protection of non-patinated, sulphide-and chloride-patinated bronze, Mater. Technol. 56 (2022) 697–704, https://doi.org/10.17222/mit.2022.641.

[10] G. Masi, J. Esvan, C. Josse, C. Chiavari, E. Bernardi, C. Martini, M.C. Bignozzi, N. Gartner, T. Kosec, L. Robbiola, Characterization of typical patinas simulating bronze corrosion in outdoor conditions, Mater. Chem. Phys. 200 (2017) 308–321, https://doi.org/10.1016/j.matchemphys.2017.07.091.

[11] M. Forslund, C. Leygraf, Humidity sorption due to deposited aerosol particles studied in situ outdoors on gold surfaces, J. Electrochem. Soc. 144 (1997) 105, https://doi.org/10.1149/1.1837371.

[12] K.J.L. Arenas, S.R. Schill, A. Malla, P.K. Hudson, Deliquescence phase transition measurements by quartz crystal microbalance frequency shifts, J. Phys. Chem. A 116 (2012) 7658–7667, https://doi.org/10.1021/jp3016722.

[13] T. Aastrup, C. Leygraf, Simultaneous infrared reflection absorption spectroscopy and quartz crystal microbalance measurements for in situ studies of the metal/atmosphere interface, J. Electrochem. Soc. 144 (1997) 2986–2990, https://doi.org/10.1149/1.1837948.

[14] A. Saftics, G.A. Prósz, B. Türk, B. Peter, S. Kurunczi, R. Horvath, In situ viscoelastic properties and chain conformations of heavily hydrated carboxymethyl dextran layers: a comparative study using OWLS and QCM-I chips coated with waveguide material, Sci. Rep. 8 (2018) 11840, https://doi.org/10.1038/s41598-018-30201-6.

[15] R.J. Horst, A. Katzourakis, B.T. Mei, S. de Beer, Design and validation of a low-cost open-source impedance based quartz crystal microbalance for electrochemical research, HardwareX 12 (2022) e00374, https://doi.org/10.1016/j.ohx.2022.e00374.

[16] V. Tsionsky, L. Daikhin, E. Gileadi, Response of the electrochemical quartz crystal microbalance for gold electrodes in the double-layer region, J. Electrochem. Soc. 143 (1996) 2240, https://doi.org/10.1149/1.1836987.

[17] V. Tsionsky, The quartz-crystal microbalance in an undergraduate laboratory experiment. I. Fundamentals and instrumentation, J. Chem. Educ. 84 (2007) 1334, https://doi.org/10.1021/ed084p1334.

[18] G. Sauerbrey, The use of quartz oscillators for weighing thin layers and for microweighing, Z. Fur. Phys. 155 (1959) 206–222, https://doi.org/10.1007/BF01337937.

[19] R. Schubert, B. Meagher, C.C. Chang, Monitoring of in situ corrosion rates in a telephone switching office in Burbank, California, J. Electrochem. Soc. 142 (1995) 3157, https://doi.org/10.1149/1.2048704.

[20] A. Krozer, B. Kasemo, Kinetics of initial oxidation of UHV prepared Zn films, Surf. Sci. Lett. 97 (1980) L339–L344, https://doi.org/10.1016/0039-6028(80)90660-3.

[21] C. Kirk Jr, E. Huber Jr, The oxidation of aluminum films in low-pressure oxygen atmospheres, Surf. Sci. 9 (1968) 217–245, https://doi.org/10.1016/0039-6028(68)90174-X.

[22] B. Kasemo, E. Törnqvist, Quartz crystal microbalance measurements of O/Ti and CO/Ti atom ratios on very thin Ti films, Surf. Sci. 77 (1978) 209–218, https://doi.org/10.1016/0039-6028(78)90002-X.

[23] T. Aastrup, M. Wadsak, M. Schreiner, C. Leygraf, Experimental in situ studies of copper exposed to humidified air, Corros. Sci. 42 (2000) 957–967, https://doi.org/10.1016/S0010-938X(99)00125-0.

[24] T. Aastrup, M. Wadsak, C. Leygraf, M. Schreiner, In situ studies of the initial atmospheric corrosion of copper influence of humidity, sulfur dioxide, ozone, and nitrogen dioxide, J. Electrochem. Soc. 147 (2000) 2543, https://doi.org/10.1149/1.1393566.

[25] H.-J. Chao, W.-C. Huang, C.-L. Chen, C.C.K. Chou, H.-M. Hung, Water adsorption vs phase transition of aerosols monitored by a quartz crystal microbalance, ACS Omega 5 (2020) 31858–31866, https://doi.org/10.1021/acsomega.0c04698.

[26] M. Tang, C.K. Chan, Y.J. Li, H. Su, Q. Ma, Z. Wu, G. Zhang, Z. Wang, M. Ge, M. Hu, H. He, X. Wang, A review of experimental techniques for aerosol hygroscopicity studies, Atmos. Chem. Phys. 19 (2019) 12631–12686, https://doi.org/10.5194/acp-19-12631-2019. ⟨https://acp.copernicus.org/articles/19/12631/2019/⟩.

[27] G. Zeng, J. Kelley, J.D. Kish, Y. Liu, Temperature-dependent deliquescent and efflorescent properties of methanesulfonate sodium studied by ATR-FTIR spectroscopy, J. Phys. Chem. A 118 (2014) 583–591, https://doi.org/10.1021/jp405896y.

[28] C. Peng, L. Chen, M. Tang, A database for deliquescence and efflorescence relative humidities of compounds with atmospheric relevance, Fundam. Res. 2 (2022) 578–587, https://doi.org/10.1016/j.fmre.2021.11.021.

[29] L. Greenspan, Humidity fixed points of binary saturated aqueous solutions, J. Res. Natl. Bur. Stand. Sect. A Phys. Chem. 81 (1977) 89, https://doi.org/10.6028/jres.081A.011.

[30] R.V. Gough, V.F. Chevrier, M.A. Tolbert, Formation of liquid water at low temperatures via the deliquescence of calcium chloride: implications for Antarctica and Mars, Planet. Space Sci. 131 (2016) 79–87, https://doi.org/10.1016/j.pss.2016.07.006.

[31] H. Strandberg, L.G. Johansson, Some aspects of the atmospheric corrosion of copper in the presence of sodium chloride, J. Electrochem. Soc., 145 (1998) Medium: X; Size, 1093–1100. https://doi.org/10.1149/1.1838422.

[32] E.J. Schindelholz, H. Cong, C. Jove Colón, S. Li, J.A. Ohlhausen, H. Moffat, Electrochemical aspects of copper atmospheric corrosion in the presence of sodium chloride, Electrochim. Acta 276 (2018), https://doi.org/10.1016/j.electacta.2018.04.184.

[33] H. Lin, G. Frankel, Atmospheric corrosion of Cu during constant deposition of NaCl, J. Electrochem. Soc. 160 (2013) C336, https://doi.org/10.1149/2.037308jes.

[34] Z. Chen, D. Persson, A. Nazarov, S. Zakipour, D. Thierry, C. Leygraf, In situ studies of the effect of CO_2 on the initial NaCl-induced atmospheric corrosion of copper, J. Electrochem. Soc. (2013), https://doi.org/10.1149/1.1984448.

[35] Z.Y. Chen, D. Persson, A. Nazarov, S. Zakipour, D. Thierry, C. Leygraf, In situ studies of the effect of CO_2 on the initial NaCl-induced atmospheric corrosion of copper, J. Electrochem. Soc. 152 (2005) B342, https://doi.org/10.1149/1.1984448.

[36] P. Yang, H. Yang, N. Wang, C. Du, S. Pang, Y. Zhang, Hygroscopicity measurement of sodium carbonate, β-alanine and internally mixed β-alanine/Na2CO3 particles by ATR-FTIR, J. Environ. Sci. 87 (2020) 250–259, https://doi.org/10.1016/j.jes.2019.07.002.

[37] M. Gobien, F. Garisto, E. Kremer, C. Medri, Sixth Case Study: Reference Data and Codes, NWMO-TR-2016–10, Nuclear Waste Management Organization, 2016.